

Density engineering via inter-condensate dipole-dipole interactions

Pranay Nayak,^{1,2} Ratheejit Ghosh,¹ and Rejish Nath¹

¹Department of Physics, Indian Institute of Science Education and Research, Pune 411 008, Maharashtra, India

²Department of Physics, Stockholm University, SE-10691 Stockholm, Sweden

(Dated: March 29, 2024)

We study the effect of inter-condensate dipole-dipole interactions in a setup consisting of physically disconnected single-species dipolar Bose-Einstein condensates. In particular, making use of the long-range and anisotropic nature of dipole-dipole interactions, we show that the density of a *target* dipolar Bose-Einstein condensate can be axially confined and engineered using a trapped *control* dipolar condensate. Increasing the number of control condensates leads to exotic ground state structures, including periodic patterns. The latter consists of single and double-peaked structures with coherence between the peaks controlled via the separation between the control condensates, thereby accessing both supersolid-like structures and incoherent arrays of density peaks.

I. INTRODUCTION

The anisotropic and long-range nature of the dipole-dipole interactions (DDIs) led to a rich physics in dipolar quantum gases [1–4]. In particular, self-confined multi-dimensional bright solitons [5–9] and ground states with density patterns [10–15] remain a focus of study in dipolar Bose-Einstein condensates (DBECs). The discovery of dipolar quantum droplets [16–21], resulting from the interplay between contact and dipolar interactions, together with the quantum stabilization [22, 23] led to a lot of exciting developments in the recent past. The most remarkable among them is the observation of incoherent arrays of droplets and droplet supersolids [24–35]. The coherence in a droplet supersolid can be probed via excitations [28, 29, 31, 36] and the quantum moment of inertia [33]. More exotic and multi-dimensional supersolids are also predicted to exist in BECs [21, 35, 37–45].

Because of the long-range nature, physically disconnected dipolar quantum systems can exhibit collective phenomena [3, 46–49]. In condensates, they include dipolar drag [50, 51], hybrid excitations [52–54], soliton complexes [55–60], and coupled density patterns [61, 62]. The inter-layer interactions can also significantly affect the stability of an atomic dipolar condensate, despite having a small atomic dipole moment ($6\mu_B$ with μ_B the Bohr magneton for a chromium atom) [63, 64]. Remarkably, a recent experiment using cold gas of dysprosium atoms ($10\mu_B$) demonstrated strong inter-layer dipolar effects by reducing the layer separations to 50 nm from typical lattice spacings of 500 nm [65], opening up new directions in the physics of dipolar gases and possibly observe various exotic bilayer phenomena [50, 53, 66–77]. The recent developments in the experiments of polar molecules with large electric dipole moments also paving alternative ways to probe inter-layer effects in dipolar gases [78, 79].

In this paper, we show that the ground state density of a *target* dipolar BEC can be engineered via inter-condensate DDIs, emerging from a set of *control* dipolar BECs. We assume all condensates are spatially disconnected, and the control BECs are spatially confined in all directions, whereas the target BEC is not axially confined. Further, we work in a regime where the corrections to the chemical potential from the quantum fluctuations or the Lee-Huang-Yang (LHY) corrections within

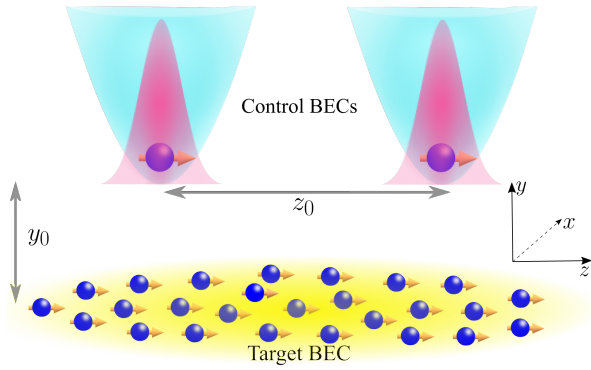


Figure 1. (color online). The schematic picture of the setup consists of three non-overlapping dipolar condensates. The two condensates in the top row, separated by a distance of z_0 , are the control BECs, whereas the bottom one is the target BEC. The target BEC is separated by a distance of y_0 from the control ones along the y -axis. The control BECs are confined in all directions, whereas the target one is axially (along z -axis) unconfined.

each condensate can be neglected [80, 81]. First, using point dipoles oriented along the axial direction, we show that a localized control dipole induces a double-well potential on the target dipole along the axial direction. It has far-reaching consequences when extended condensates. For instance, because of the double-well potential, a control dipolar condensate axially confines a target BEC and creates a density minimum at its center. The control over the resultant density structure of the target BEC, i.e., its axial width and the peak density, can be easily achieved by varying the trap aspect ratio of the control BEC.

Increasing the number of control BECs imprints nontrivial density patterns on the target condensate. Strikingly, such density patterns can be engineered in a controlled manner, as we demonstrate. For instance, in a setup consisting of two control BECs, the ground state of the target condensate undergoes a structural transition from a three-peaked to a four-peaked pattern when the separation between the control BECs is varied. Interestingly, a periodic array of control BECs induces an effective periodic potential on the target BEC, forming various periodic density patterns.

Three-dimensional numerical analysis of the coupled non-local Gross-Pitaevskii equations reveals a periodic arrangement of single and double-peaked periodic structures forming coherent (supersolid-like) and incoherent density waves. They contrast highly with the supersolids stabilized by the LHY correction and are fundamentally different. But similar to the immiscible double-supersolids in binary dipolar condensates in which one component supports the density modulation in the other component [82, 83] for which the quantum stabilization from LHY corrections is not required. Strikingly, the periodic structure we discuss is at the low-density regime in high contrast to the high-density droplet arrays in dipolar condensates. We further show that the overlap between the peaks and, hence, the superfluidity or the coherence between them can be controlled by tuning the separation between the control BECs.

The paper is structured as follows. The setup and model are introduced in Sec. II. In Sec. III B, we discuss the axial confinement of the target dipolar BEC using a single control BEC. The density engineering using two control BECs is discussed in Sec. IV. The formation of periodic density peaks, including the supersolids in the target BEC due to an array of control BECs, is discussed in Sec. V. Finally, we summarize and provide an outlook in Sec. VI.

II. SETUP AND MODEL

The setup consists of M spatially disconnected dipolar condensates where one is a target BEC, and the rest are control BECs. The control BECs are confined in all three directions, whereas the target one is not axially confined, but the radial trapping potential is the same as that of the control ones. A schematic setup for $M = 3$ is shown in Fig. 1. The two condensates in the upper row are the control BECs, and the bottom one, separated by a distance of y_0 in the transverse y -direction, is the target BEC. Let N_t and N_c be the number of bosons in each target and control BECs, respectively. Each boson has a mass m and magnetic dipole moment d (results are equally valid for electric dipoles) oriented along z axis [see Fig. 1]. At very low temperatures, the system is described in the mean field by coupled non-local Gross-Pitaevskii equations (NLGPEs),

$$i\hbar \frac{\partial}{\partial t} \psi_j(\mathbf{r}, t) = \left(-\frac{\hbar^2}{2m} \nabla^2 + V_j(\mathbf{r}) + g N_j |\psi_j(\mathbf{r}, t)|^2 + \sum_{i=1}^M N_i \int d^3 r' V_d(r - r') |\psi_i(\mathbf{r}', t)|^2 \right) \psi_j(\mathbf{r}, t) \quad (1)$$

where ψ_j is the wavefunction of the j th condensate satisfying $\int |\psi_j(\mathbf{r})|^2 d^3 r = 1$, $N_j \in \{N_t, N_c\}$ and $V_j(\mathbf{r})$ is its external potential. The trapping potential experienced by a control BEC is $V_j(\mathbf{r}) = m\omega_\perp^2[x^2 + (y - y_0)^2]/2 + m\omega_z^2(z - z_j)^2/2$, where ω_\perp and ω_z are the trapping frequencies along the radial and axial directions and that of the target BEC is $m\omega_\perp^2(x^2 + y^2)/2$. The parameter $g = 4\pi\hbar^2 a_s/m$ quantifies the contact interaction strength with $a_s > 0$ being the s -wave scattering length. The dipolar potential is $V_d(\mathbf{r}) = g_d(1 - 3\cos^2\theta)/r^3$, where

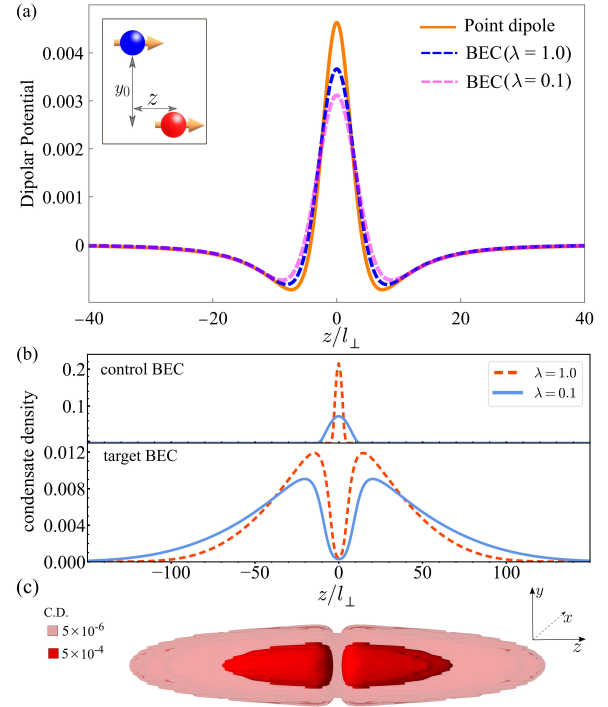


Figure 2. (color online). (a) The dipolar potential experienced by the target dipole due to a control dipole, $V_d^{\text{tar}}(z/l_\perp)^3/g_d$ as in Eq. (3) (solid line) and due to a control BEC, $\tilde{V}_d^{\text{tar}}(x = 0, y = 0, z/l_\perp)^3/g_d$, as in Eq. (4) (dashed lines) for $y_0 = 6l_\perp$ and the aspect ratio $\lambda = 0.1$ and 1. (b) The integrated column density ($l_\perp \int \int dx dy |\psi_j(\mathbf{r})|^2$) along the z -axis of control ($j = c$) and target ($j = t$) BECs for $y_0 = 6l_\perp$, $\tilde{g}_j = 210$, and $\tilde{g}_{dj} = 50$, which corresponds to $N_c = N_t = 29000$ (Cr), 3700 (Er) and 1900 (Dy), and $a_s/a_0 = 15.2$ (Cr) [85], 66.5 (Er) [25] and 131.8 (Dy) [27], where a_0 is the Bohr radius. Dashed lines are for $\lambda = 1$, and solid lines are for $\lambda = 0.1$. (c) The iso-surface density plot of the target BEC for $\lambda = 1$. C.D. stands for condensate density $l_\perp^3 |\psi_t(\mathbf{r})|^2$. In the numerics, the grid extensions used are $(-x_{\max}, x_{\max})$, $(-y_{\max}, y_{\max})$ and $(-z_{\max}, z_{\max})$ with $x_{\max} = y_{\max} = 25l_\perp$, and $z_{\max} = 200l_\perp$, which is much larger than the size of the condensate. The cutoffs used for the dipolar potential are $R = 22.5l_\perp$ and $Z = 180l_\perp$.

$g_d = \mu_0 d^2 / 4\pi$ with μ_0 being the magnetic permeability and θ is the angle between the dipole moment and the radial vector \mathbf{r} joining the two dipoles. We introduce the dimensionless parameters $\tilde{g}_j = gN_j/\hbar\omega_\perp l_\perp^3$ and $\tilde{g}_{dj} = g_d N_j/\hbar\omega_\perp l_\perp^3$ to quantify the interaction strengths, where $l_\perp = \sqrt{\hbar/m\omega_\perp}$. The contact interaction strength g is taken sufficiently large to ensure each condensate is dynamically stable, which also rules out the self-trapping of the target BEC along the axial direction [55]. The ground states of the complete system are obtained by solving the coupled three-dimensional NLGPEs in Eq. (1) via imaginary time evolution as detailed in [84].

Considering our setup involves cylindrical geometries, we use a truncated dipolar potential [14, 86], $V_d^{\text{cut}}(\mathbf{r}) = g_d(1 - 3\cos^2\theta)/r^3$ when $|z| < Z$ and $\rho < R$, and zero otherwise. Further, the DDIs in Eq. (1) are tackled using the convolution

theorem, which requires the Fourier transform of $V_d^{\text{cut}}(\mathbf{r})$ [14],

$$\tilde{V}_d^{\text{cut}}(\mathbf{k}) = 4\pi g_d \left[\frac{3 \cos^2 \theta_k - 1}{3} + e^{-Zk_p} \left(\sin^2 \theta_k \cos k_z Z - \frac{\sin 2\theta_k \sin k_z Z}{2} \right) - \int_R^\infty \rho d\rho \int_0^Z dz \frac{\rho^2 - 2z^2}{(\rho^2 + z^2)^{5/2}} J_0(k_\rho \rho) \cos k_z z \right] \quad (2)$$

where, $k_\rho = \sqrt{k_x^2 + k_y^2}$, $\cos^2 \theta_k = k_z^2 / (k_\rho^2 + k_z^2)$, and $J_0(\cdot)$ is the zeroth-order Bessel function. The cutoff values Z and R are taken such that they cover the complete system in all directions.

III. AXIAL CONFINEMENT

First, we discuss how a control BEC can axially confine the target BEC via the inter-tube DDIs. A qualitative picture can be easily obtained by considering points dipoles as follows.

A. Point dipoles

The schematic diagram of a pair of point dipoles is shown in the inset of Fig. 2(a). The control dipole is localized at the coordinates $y = y_0$ and $z = 0$, whereas the target dipole at $y = 0$ is free to move along the axial z -direction. The dipolar potential experienced by the target dipole along the z -axis is

$$V_d^{\text{tar}}(z) = g_d \frac{(y_0^2 - 2z^2)}{(y_0^2 + z^2)^{5/2}}. \quad (3)$$

Since two parallel dipoles in side-by-side configuration repel each other maximally, $V_d^{\text{tar}}(z)$ exhibits a finite repulsive barrier centered at $z = 0$. As the separation z becomes larger, the dipoles are in a head-to-tail configuration, and the dipolar potential is attractive but decaying as $\sim -2g_d/z^3$. This attractive nature of $V_d^{\text{tar}}(z)$ at large z axially confines the target dipole. The change from repulsive to attractive behavior of $V_d^{\text{tar}}(z)$ results in a local minimum on either side of $z = 0$. Effectively, the control dipole induces a double-well potential on the target dipole, as shown (solid line) in Fig. 2(a).

B. Dipolar condensates

At this point, we consider dipolar BECs instead of point dipoles. As the control BEC is confined in all directions, it acts as a giant dipole, and we expect the target dipole to experience a qualitatively similar potential as that of point dipoles. To verify that, we calculate the (mean-field) dipolar potential induced by a dipole distributed over the density of the control BEC on the target dipole, i.e.,

$$\tilde{V}_d^{\text{tar}}(\mathbf{r}) = \int d^3 r' V_d(\mathbf{r} - \mathbf{r}') n_c(\mathbf{r}'), \quad (4)$$

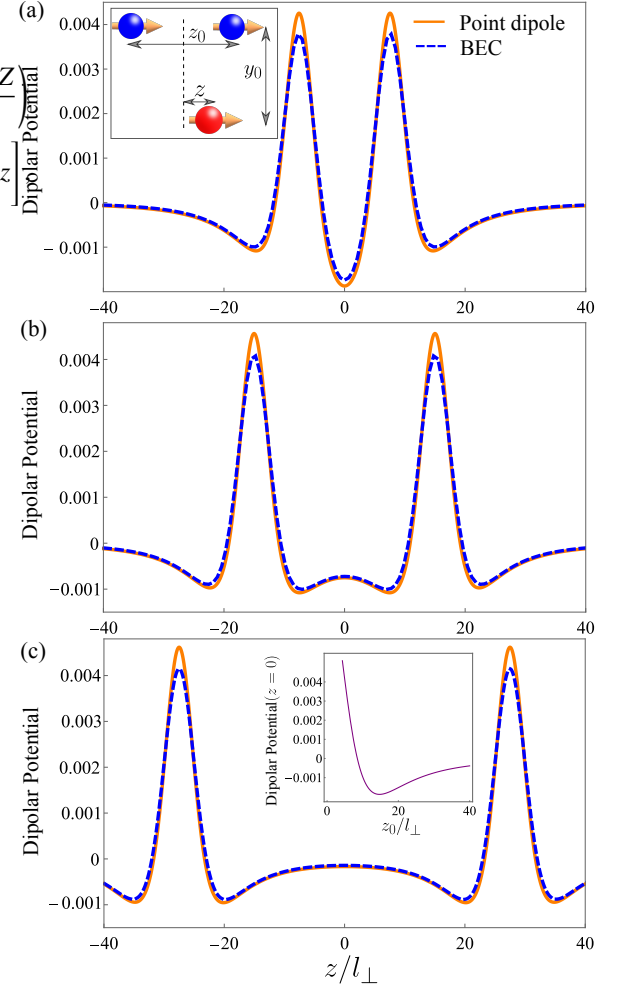


Figure 3. (color online). The inset of (a) shows the schematic diagram of the three-point dipole setup. The two control dipoles (blue) are shown on the top row, localized and separated by z_0 . The dipole in the bottom (red) is the target one. The dipolar potential experienced by the target dipole due to two localized control dipoles, $V_d^{\text{tar}}(z) l_{\perp}^3/g_d$ as in Eq. (5) (solid lines) and the same due to two control BECs for $y_0 = 6l_{\perp}$, (a) $z_0 = 15l_{\perp}$, (b) $z_0 = 30l_{\perp}$ and (c) $z_0 = 55l_{\perp}$. The inset of (c) shows $V_d^{\text{tar}}(z = 0) l_{\perp}^3/g_d$ as a function of z_0 , exhibiting a non-monotonous behavior. The trap aspect ratio of control BECs is $\lambda = 0.33$.

where $n_c(\mathbf{r}) = |\psi_c(\mathbf{r})|^2$ is the density of the control BEC. In Fig. 2(a), we show $\tilde{V}_d^{\text{tar}}(x = 0, y = 0, z)$ and is found to be similar to the double-well potential generated by a point dipole. The larger the value of λ , the closer the potential to the point dipole case. The actual potential on the target BEC is N_c times the potential $\tilde{V}_d^{\text{tar}}(\mathbf{r})$.

As expected, the ground state of the target condensate is axially confined by the inter-tube DDIs. In Fig. 2(b), we show the results for two values of the control BEC's trap aspect ratio $\lambda = \omega_z/\omega_{\perp}$ and $N_c = N_t$. The integrated column density of the control BEC is shown at the top, and that of the target BEC is shown at the bottom. The repulsive barrier in $V_d^{\text{tar}}(z)$ creates a density minimum on the target BEC centered at $z = 0$, leading to a two-peaked structure, as shown in Figs. 2(b) and 2(c).

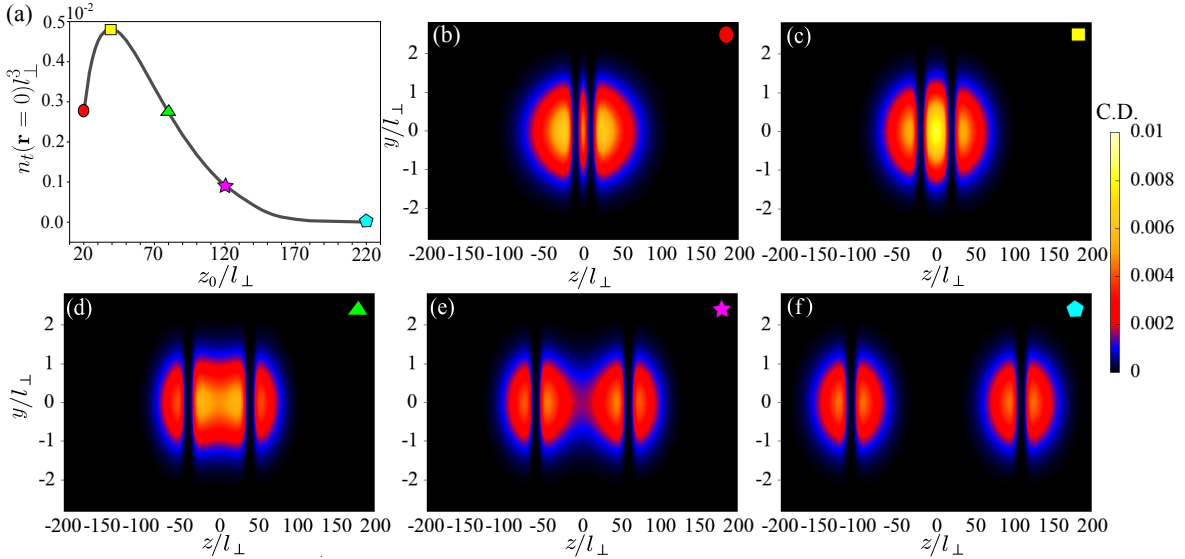


Figure 4. (color online). (a) The central density, $n_t(\mathbf{r} = 0) = |\psi_t(\mathbf{r} = 0)|^2$ of the target BEC as a function of z_0 . (b)-(f) shows the integrated ground state density ($l_{\perp}^2 \int dx |\psi_t(\mathbf{r})|^2$) of the target BEC for $z_0 = 20l_{\perp}$, $z_0 = 40l_{\perp}$, $z_0 = 80l_{\perp}$, $z_0 = 120l_{\perp}$ and $z_0 = 220l_{\perp}$, respectively and $\lambda = 0.33$. (b)-(d) exhibit three peaks, whereas (e)-(f) possess four peaks. The other parameters are same as in Fig. 2. C.D. stands for the condensate density $l_{\perp}^2 \int dx |\psi_t(\mathbf{r})|^2$. In the numerics, the grid extensions used are $(-x_{\max}, x_{\max})$, $(-y_{\max}, y_{\max})$ and $(-z_{\max}, z_{\max})$ with $x_{\max} = y_{\max} = 30l_{\perp}$, and $z_{\max} = 300l_{\perp}$. The cutoffs used for the dipolar potential are $R = 27l_{\perp}$ and $Z = 270l_{\perp}$.

The target BEC's axial width and peak density can be easily controlled by adjusting λ . The tighter the axial confinement of the control BEC, the larger the peak density and the lesser the axial width of the target BEC. The number of atoms required for the state-of-the-art dipolar BECs such as chromium (Cr) [87, 88], erbium (Er) [89–91] and dysprosium (Dy) [92] are provided in the caption of Fig. 2.

IV. DENSITY ENGINEERING OF THE TARGET BEC

Increasing the number of control BECs can lead to exotic density patterns in the target BEC. To demonstrate that, we consider two control BECs as depicted in Fig. 1. As we discuss below, the density patterns depend critically on the separation z_0 between the two control BECs. To get an intuitive picture, we again look at the dipolar potential of three-point dipoles in a geometry identical to the BEC setup in Fig. 1. The dipolar potential experienced by the target dipole (bottom) due to two control dipoles (top) localized at $\pm z_0/2$ is,

$$V_d^{\text{tar}}(z) = 16g_d \frac{2y_0^2 - (z_0 - 2z)^2}{[4y_0^2 + (z_0 - 2z)^2]^{5/2}} + \frac{2y_0^2 - (z_0 + 2z)^2}{[4y_0^2 + (z_0 + 2z)^2]^{5/2}}. \quad (5)$$

In Fig. 3, we show $V_d^{\text{tar}}(z)$ as a function of z for three different values of z_0 . The potential has two maxima at $\pm z_0/2$ due to the side-by-side repulsion from the control dipoles. A minimum is on either side of each maximum, with the total number of minima depending on z_0 . For small values of z_0 , $V_d^{\text{tar}}(z)$ exhibits a minimum at $z = 0$ [see Fig. 3(a)] and as z_0 increases, the minimum gets deeper. A further increase in z_0 , the minimum turns into a local maximum, resulting in a pair

of minima on either side of $z = 0$ [see Fig. 3(b)]. A larger z_0 increases the width of the central region, pushing the minima away from each other, resulting in a pair of double-well potentials as shown in Fig. 3(c). Thus, each control dipole induces a double-well potential on the target dipole for a large separation between them. The nature of potential at $z = 0$ also depends critically on z_0 as shown in the inset of Fig. 3(c), which exhibits a non-monotonous behavior. In short, the dipolar potential experienced by the target dipole can be engineered by varying the separation between the two control dipoles. In particular, $V_d^{\text{tar}}(z)$ exhibits three local minima for small z_0 and four minima as z_0 becomes larger. When considering BEC, we use Eq. (4) to calculate the contribution from each control BEC and sum over them. The resulting potential for the condensates scaled by g_d/l_{\perp}^3 is also shown in Fig. 3 for $\lambda = 0.33$, and is almost identical to that of point dipoles.

The effect of varying the separation z_0 between the control BECs on the ground state of the target BEC (n_t^{tar}) is shown in Fig. 4. As before, the inter-condensate DDIs axially confine the target condensate. In Fig. 4(a), we plot the central density of the target BEC as a function of z_0 , which exhibits a non-monotonous behavior possessing a maximum, as expected from the spatial dependence of $V_d^{\text{tar}}(z = 0)$ shown in the inset of Fig. 3(c). For sufficiently small z_0 , we get a three-peak structure with a sharper peak at the center [see Fig. 4(b)]. Upon increasing z_0 , the central peak gets broader and denser [Fig. 4(c)] since the minimum of the potential at $z = 0$ gets deeper. Above a particular value, the behavior changes, and an increment in z_0 starts to reduce the central density. As $V_d^{\text{tar}}(z = 0)$ becomes a local maximum, the central density lobe develops a modulation as seen in Fig. 4(d), which eventually breaks into two peaks at large z_0 [see Figs. 4(e) and

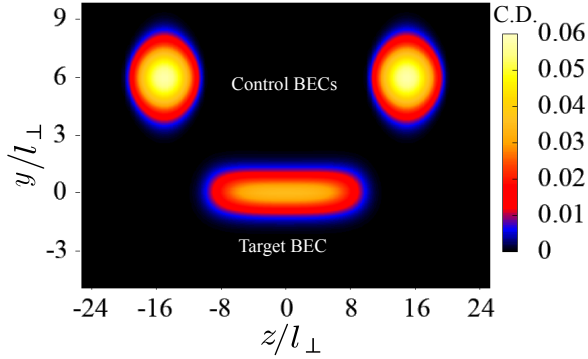


Figure 5. (color online). The integrated condensate density ($\int dx |\psi_j(\mathbf{r})|^2$) of control ($j = c$) and target ($j = t$) BECs for $y_0 = 6l_\perp$, $z_0 = 30l_\perp$ and $\lambda = 1$. For control BECs, $\tilde{g}_{dt} = 200$ and $\tilde{g}_t = 840$, and for the target BEC, $\tilde{g}_{dc} = 10$ and $\tilde{g}_c = 42$ and together, they correspond to $\{N_c = 116000, N_t = 5800\}$ for Cr, $\{N_c = 14770, N_t = 740\}$ for Er and $\{N_c = 7500, N_t = 380\}$ for Dy. C.D. stands for condensate density $\int dx |\psi_t(\mathbf{r})|^2$. In the numerics, the grid extensions used are $(-x_{\max}, x_{\max})$, $(-y_{\max}, y_{\max})$ and $(-z_{\max}, z_{\max})$ with $x_{\max} = y_{\max} = 30l_\perp$, and $z_{\max} = 150l_\perp$. The cutoffs used for the dipolar potential are $R = 27l_\perp$ and $Z = 135l_\perp$.

4(f)]. Finally, at large z_0 , a pair of semi-ellipsoid condensates is formed on either side of $z = 0$, leading to a four-peaked ground state density profile. The separation between them can be made larger by incrementing z_0 further.

So far, the atom number is the same for target and control BECs. Reducing the number of atoms in the target BEC leads to a single ellipsoid-shaped condensate formed in the region between the control condensates, as shown in Fig. 5. In Fig. 5, we show the densities of both the control (two peaks on the top) and target (bottom) condensates.

V. PERIODIC PATTERNS

Finally, we show that having an array of control BECs can imprint various periodic patterns on the ground state density of the target BEC, including supersolid-like structures. In Fig. 6, we show the potential experienced by the target dipole from a periodic array of six control dipoles for different z_0 , where z_0 is now the separation between the adjacent control dipoles. For smaller values of z_0 , the potential has seven local minima [see Fig. 6(a) for $z_0 = 12l_\perp$], with inner minima being narrower than the outer ones. As z_0 increases, the inner minima get broader, and the outer ones get narrower [see Fig. 6(b) for $z_0 = 20l_\perp$]. When the separation is more significant, each control dipole induces a double-well potential centered around its location. Hence, a maximum of twelve minima emerges in the dipolar-potential as shown in Fig. 6(c), for $z_0 = 100l_\perp$.

The numerically obtained ground state densities of the target BEC are shown in Fig. 7. For sufficiently small z_0 , we see a seven-peaked structure, with outer density lobes significantly broader and higher in density than the inner ones [see Fig. 7(a) for $z_0 = 12l_\perp$]. It is expected since the inner potential minima

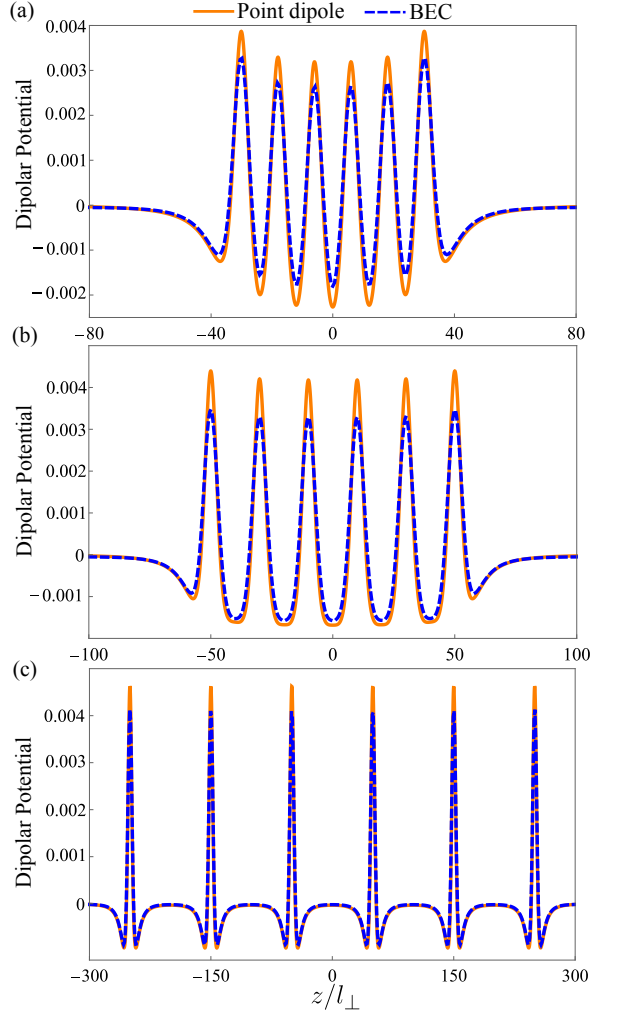


Figure 6. (color online). The dipolar potential $V_d^{\text{tar}}(z)l_\perp^3/g_d$ experienced by the target dipole due to six localized control dipoles (solid line) for $y_0 = 6l_\perp$, (a) $z_0 = 12l_\perp$, (b) $z_0 = 20l_\perp$ and (b) $z_0 = 100l_\perp$, where z_0 is the separation between adjacent control dipoles. The same due to the control BECs for $\lambda = 1$ is shown by dashed line. At large z_0 , as in (c), the total potential can be seen as an array of double-well potentials.

are narrower, and increasing the density there costs more energy. Increasing z_0 leads to a structural modification, where the inner lobes get broader and denser than those at the edges [see Figs. 7(b) and 7(c) for $z_0 = 20l_\perp$ and $z_0 = 40l_\perp$]. As z_0 increases further, the inner density lobes develop density modulation, [see Figs. 7(d) for $z_0 = 60l_\perp$] and eventually becomes double-peaked pattern at large values of z_0 as shown in Figs. 7(e) and 7(f) for $z_0 = 80l_\perp$ and $z_0 = 150l_\perp$, respectively.

At this point, we quantify the coherence between the density lobes using Leggett's upper bound of the superfluid fraction [93]:

$$f_s = (2L)^2 \left[\int_{-L}^L dz \tilde{n}(z) \int_{-L}^L \frac{dz}{\tilde{n}(z)} \right]^{-1}, \quad (6)$$

where $\tilde{n}(z)$ is the column density obtained after the radial in-

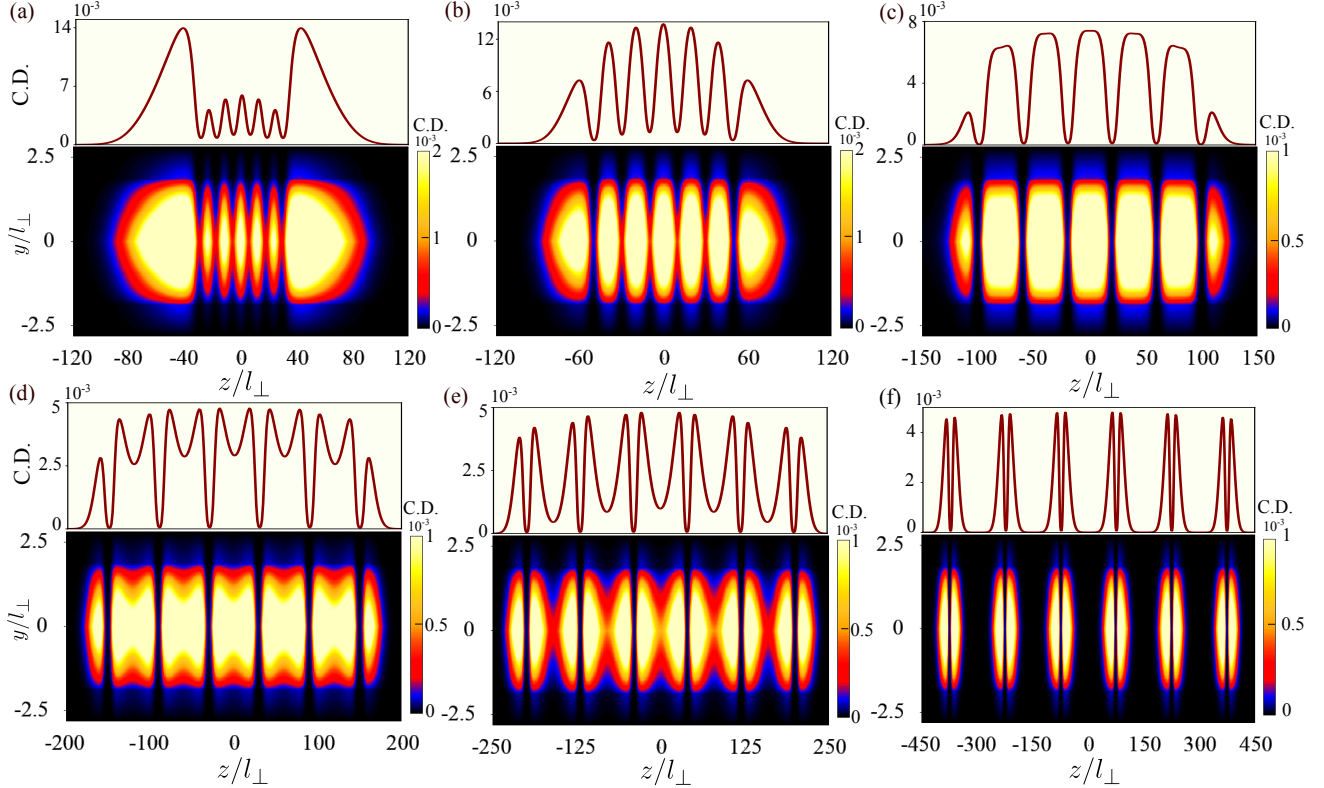


Figure 7. (color online). The integrated condensate density ($\int dx |\psi_j(\mathbf{r})|^2$) of the target BEC for different values of z_0 in the presence of a periodic array of six control BECs for $y_0 = 6l_{\perp}$, (a) $z_0 = 12l_{\perp}$, (b) $z_0 = 20l_{\perp}$, (c) $z_0 = 40l_{\perp}$, (d) $z_0 = 60l_{\perp}$, (e) $z_0 = 80l_{\perp}$, and (f) $z_0 = 150l_{\perp}$. The other parameters are $\lambda = 1$, $\tilde{g}_{dt} = \tilde{g}_{dc} = 50$ and $\tilde{g}_t = \tilde{g}_c = 210$, and they are the same as for Fig. 2. (a)-(e) are supersolids, whereas (f) is an incoherent array of density peaks. C.D. stands for condensate density $\int dx |\psi_j(\mathbf{r})|^2$. In the numerics, the grid extensions used are $(-x_{\max}, x_{\max})$, $(-y_{\max}, y_{\max})$ and $(-z_{\max}, z_{\max})$ with $x_{\max} = y_{\max} = 30l_{\perp}$, and (a)-(b) $z_{\max} = 150l_{\perp}$, (c) $z_{\max} = 300l_{\perp}$, (d) $z_{\max} = 350l_{\perp}$, (e) $z_{\max} = 450l_{\perp}$ and (f) $z_{\max} = 760l_{\perp}$. The cutoffs used for the dipolar potential are $R = 27l_{\perp}$, (a)-(b) $Z = 135l_{\perp}$, (c) $Z = 270l_{\perp}$, (d) $Z = 315l_{\perp}$, (e) $Z = 405l_{\perp}$ and (f) $Z = 684l_{\perp}$.

egration, and the length $2L$ encloses the central region. For Figs. 7(a)-7(d), the distance $2L$ is defined such that the three density lobes in the center are covered, whereas, for the last three patterns, the length $2L$ includes the size of a pair of double-peak structure at the center. We see that f_s exhibits a non-trivial dependence on z_0 . The pattern in Fig. 7(a) for $z_0 = 12l_{\perp}$ has $f_s = 0.68$. As the separation between the adjacent control BECs increases, f_s decreases. For instance, increasing z_0 to $20l_{\perp}$ [Fig. 7(b)] makes $f_s = 0.51$ and for $z_0 = 40l_{\perp}$ [Fig. 7(c)], f_s further decreases to 0.195. Once the density modulation develops in the inner density lobes, f_s increases with an increase in z_0 , particularly, $f_s = 0.227$ and $f_s = 0.344$ for $z_0 = 60l_{\perp}$ [Fig. 7(d)] and $z_0 = 80l_{\perp}$ [Fig. 7(e)], respectively. As the modulation grows into a nodal plane at large z_0 , f_s decreases again with increase in z_0 , and for Fig. 7(f), $f_s = 0.006$ with $z_0 = 150l_{\perp}$. To conclude this section, for the patterns in Figs. 7(a)-7(e), $f_s > 0.1$, indicating a sufficient superfluid flow between the density lobes to establish the coherence and hence, a supersolid-like pattern, whereas the state shown in Fig. 7(f) is an incoherent array of density peaks.

VI. SUMMARY AND OUTLOOK

To summarize, utilizing the inter-condensate DDIs, we showed that the density of a target BEC can be axially confined and engineered using a single control BEC. When extended to multiple control BECs, exotic density patterns are formed. Each control BEC induces a double-well-like potential on the target BEC, and the total potential on the target BEC depends critically on the separation between the control BECs. As shown, it is possible to engineer a supersolid-like pattern on the target BEC, i.e., without the support of quantum stabilization emerging from the LHY corrections. Further, we observed a structural crossover between patterns of two periodicities when the separation between the adjacent control BECs is varied.

Our studies also open up several perspectives. Apart from the density engineering of the target condensate, there is a possibility of manipulating the quantum state of other dipolar systems, such as polar molecules or Rydberg atoms, using dipolar condensates placed significantly far from the target system. Since hybrid systems of polar molecules and Rydberg atoms are gaining a lot of attention, based on our studies, the bound states of polar molecules and Rydberg atoms stabilized

by dipolar interactions may be feasible and will be explored in the future [94].

VII. ACKNOWLEDGEMENTS

We thank C. Mishra for the discussions during the initial stages of the work. We acknowledge National Supercomputing Mission (NSM) for providing computing resources of

“PARAM Brahma” at IISER Pune, which is implemented by C-DAC and supported by the Ministry of Electronics and Information Technology (MeitY) and Department of Science and Technology (DST), Government of India. P. N. acknowledges the funding from DST India through an INSPIRE scholarship. R.N. further acknowledges DST-SERB for Swarnajayanti fellowship File No. SB/SJF/2020-21/19, and the MATRICS grant (MTR/2022/000454) from SERB, Government of India.

-
- [1] M. A. Baranov, *Physics Reports* **464**, 71 (2008).
 - [2] T. Lahaye, C. Menotti, L. Santos, M. Lewenstein, and T. Pfau, *Reports on Progress in Physics* **72**, 126401 (2009).
 - [3] M. A. Baranov, M. Dalmonte, G. Pupillo, and P. Zoller, *Chemical Reviews* **112**, 5012 (2012).
 - [4] N. Defenu, T. Donner, T. Macrì, G. Pagano, S. Ruffo, and A. Trombettoni, *Rev. Mod. Phys.* **95**, 035002 (2023).
 - [5] P. Pedri and L. Santos, *Phys. Rev. Lett.* **95**, 200404 (2005).
 - [6] I. Tikhonенков, B. A. Malomed, and A. Vardi, *Phys. Rev. Lett.* **100**, 090406 (2008).
 - [7] R. Nath, P. Pedri, and L. Santos, *Phys. Rev. Lett.* **102**, 050401 (2009).
 - [8] M. Raghuandan, C. Mishra, K. Łakomy, P. Pedri, L. Santos, and R. Nath, *Phys. Rev. A* **92**, 013637 (2015).
 - [9] C. Mishra and R. Nath, *Phys. Rev. A* **94**, 033633 (2016).
 - [10] K. Góral, K. Rzążewski, and T. Pfau, *Phys. Rev. A* **61**, 051601 (2000).
 - [11] O. Dutta and P. Meystre, *Phys. Rev. A* **75**, 053604 (2007).
 - [12] S. Ronen, D. C. E. Bortolotti, and J. L. Bohn, *Phys. Rev. Lett.* **98**, 030406 (2007).
 - [13] R. M. Wilson, S. Ronen, J. L. Bohn, and H. Pu, *Phys. Rev. Lett.* **100**, 245302 (2008).
 - [14] H.-Y. Lu, H. Lu, J.-N. Zhang, R.-Z. Qiu, H. Pu, and S. Yi, *Phys. Rev. A* **82**, 023622 (2010).
 - [15] L. Chomaz, I. Ferrier-Barbut, F. Ferlaino, B. Laburthe-Tolra, B. L. Lev, and T. Pfau, *Reports on Progress in Physics* **86**, 026401 (2023).
 - [16] H. Kadau, M. Schmitt, M. Wenzel, C. Wink, T. Maier, I. Ferrier-Barbut, and T. Pfau, *Nature* **530**, 194 (2016).
 - [17] I. Ferrier-Barbut, H. Kadau, M. Schmitt, M. Wenzel, and T. Pfau, *Phys. Rev. Lett.* **116**, 215301 (2016).
 - [18] L. Chomaz, S. Baier, D. Petter, M. J. Mark, F. Wächtler, L. Santos, and F. Ferlaino, *Phys. Rev. X* **6**, 041039 (2016).
 - [19] M. Schmitt, M. Wenzel, F. Böttcher, I. Ferrier-Barbut, and T. Pfau, *Nature* **539**, 259 (2016).
 - [20] D. Baillie, R. M. Wilson, R. N. Bisset, and P. B. Blakie, *Phys. Rev. A* **94**, 021602 (2016).
 - [21] M. Schmidt, L. Lassablière, G. Quéméner, and T. Langen, *Phys. Rev. Res.* **4**, 013235 (2022).
 - [22] F. Wächtler and L. Santos, *Phys. Rev. A* **93**, 061603 (2016).
 - [23] C. Mishra, L. Santos, and R. Nath, *Phys. Rev. Lett.* **124**, 073402 (2020).
 - [24] M. Sohmen, C. Politi, L. Klaus, L. Chomaz, M. J. Mark, M. A. Norcia, and F. Ferlaino, *Phys. Rev. Lett.* **126**, 233401 (2021).
 - [25] L. Chomaz, D. Petter, P. Ilzhöfer, G. Natale, A. Trautmann, C. Politi, G. Durastante, R. M. W. van Bijnen, A. Patscheider, M. Sohmen, M. J. Mark, and F. Ferlaino, *Phys. Rev. X* **9**, 021012 (2019).
 - [26] L. Tanzi, E. Lucioni, F. Famà, J. Catani, A. Fioretti, C. Gabbanini, R. N. Bisset, L. Santos, and G. Modugno, *Phys. Rev. Lett.* **122**, 130405 (2019).
 - [27] F. Böttcher, J.-N. Schmidt, M. Wenzel, J. Hertkorn, M. Guo, T. Langen, and T. Pfau, *Phys. Rev. X* **9**, 011051 (2019).
 - [28] M. Guo, F. Böttcher, J. Hertkorn, J.-N. Schmidt, M. Wenzel, H. P. Büchler, T. Langen, and T. Pfau, *Nature* **574**, 386 (2019).
 - [29] L. Tanzi, S. M. Rocuzzo, E. Lucioni, F. Famà, A. Fioretti, C. Gabbanini, G. Modugno, A. Recati, and S. Stringari, *Nature* **574**, 382 (2019).
 - [30] P. Ilzhöfer, M. Sohmen, G. Durastante, C. Politi, A. Trautmann, G. Natale, G. Morpurgo, T. Giamarchi, L. Chomaz, M. J. Mark, and F. Ferlaino, *Nature Physics* **17**, 356 (2021).
 - [31] G. Natale, R. M. W. van Bijnen, A. Patscheider, D. Petter, M. J. Mark, L. Chomaz, and F. Ferlaino, *Phys. Rev. Lett.* **123**, 050402 (2019).
 - [32] J. Hertkorn, J.-N. Schmidt, F. Böttcher, M. Guo, M. Schmidt, K. S. H. Ng, S. D. Graham, H. P. Büchler, T. Langen, M. Zwierlein, and T. Pfau, *Phys. Rev. X* **11**, 011037 (2021).
 - [33] L. Tanzi, J. G. Maloberti, G. Biagioni, A. Fioretti, C. Gabbanini, and G. Modugno, *Science* **371**, 1162 (2021).
 - [34] M. A. Norcia, C. Politi, L. Klaus, E. Poli, M. Sohmen, M. J. Mark, R. N. Bisset, L. Santos, and F. Ferlaino, *Nature* **596**, 357 (2021).
 - [35] T. Bland, E. Poli, C. Politi, L. Klaus, M. A. Norcia, F. Ferlaino, L. Santos, and R. N. Bisset, *Phys. Rev. Lett.* **128**, 195302 (2022).
 - [36] K. Mukherjee and S. M. Reimann, *Phys. Rev. A* **107**, 043319 (2023).
 - [37] N. Henkel, R. Nath, and T. Pohl, *Phys. Rev. Lett.* **104**, 195302 (2010).
 - [38] Z.-K. Lu, Y. Li, D. S. Petrov, and G. V. Shlyapnikov, *Phys. Rev. Lett.* **115**, 075303 (2015).
 - [39] D. Baillie and P. B. Blakie, *Phys. Rev. Lett.* **121**, 195301 (2018).
 - [40] J. Hertkorn, J.-N. Schmidt, M. Guo, F. Böttcher, K. S. H. Ng, S. D. Graham, P. Uerlings, T. Langen, M. Zwierlein, and T. Pfau, *Phys. Rev. Res.* **3**, 033125 (2021).
 - [41] E. Poli, T. Bland, C. Politi, L. Klaus, M. A. Norcia, F. Ferlaino, R. N. Bisset, and L. Santos, *Phys. Rev. A* **104**, 063307 (2021).
 - [42] L. E. Young-S. and S. K. Adhikari, *Phys. Rev. A* **105**, 033311 (2022).
 - [43] R. Ghosh, C. Mishra, L. Santos, and R. Nath, *Phys. Rev. A* **106**, 063318 (2022).
 - [44] K. Mukherjee, M. N. Tengstrand, T. A. Cardinale, and S. M. Reimann, *Phys. Rev. A* **108**, 023302 (2023).
 - [45] C. Mishra, S. Ostermann, F. Mivehvar, and B. P. Venkatesh, *Phys. Rev. A* **107**, 023312 (2023).
 - [46] C. Kollath, J. S. Meyer, and T. Giamarchi, *Phys. Rev. Lett.* **100**, 130403 (2008).

- [47] Y.-P. Huang and D.-W. Wang, *Phys. Rev. A* **80**, 053610 (2009).
- [48] R. M. Lutchyn, E. Rossi, and S. Das Sarma, *Phys. Rev. A* **82**, 061604 (2010).
- [49] M. Knap, E. Berg, M. Ganahl, and E. Demler, *Phys. Rev. B* **86**, 064501 (2012).
- [50] N. Matveeva, A. Recati, and S. Stringari, *The European Physical Journal D* **65**, 219 (2011).
- [51] A. Gallemi, M. Guilleumas, R. Mayol, and M. Pi, *Journal of Physics: Conference Series* **497**, 012035 (2014).
- [52] M. Klawunn and L. Santos, *Phys. Rev. A* **80**, 013611 (2009).
- [53] C.-C. Huang and W.-C. Wu, *Phys. Rev. A* **82**, 053612 (2010).
- [54] A. Maluckov, G. Gligorić, L. c. v. Hadžievski, B. A. Malomed, and T. Pfau, *Phys. Rev. A* **87**, 023623 (2013).
- [55] R. Nath, P. Pedri, and L. Santos, *Phys. Rev. A* **76**, 013606 (2007).
- [56] P. Köberle and G. Wunner, *Phys. Rev. A* **80**, 063601 (2009).
- [57] K. Łakomy, R. Nath, and L. Santos, *Phys. Rev. A* **86**, 013610 (2012).
- [58] K. Łakomy, R. Nath, and L. Santos, *Phys. Rev. A* **85**, 033618 (2012).
- [59] K. M. Elhadj, A. Boudjemâa, and U. Al-Khawaja, *Physica Scripta* **94**, 085402 (2019).
- [60] G. Hegde, P. Nayak, R. Ghosh, and R. Nath, *J. Phys. B: At., Mol. Opt. Phys.* **54**, 205301 (2021).
- [61] K. Łakomy, R. Nath, and L. Santos, *Phys. Rev. A* **86**, 023620 (2012).
- [62] S. Nadiger, S. M. Jose, R. Ghosh, I. Kaur, and R. Nath, “Stripe and checkerboard patterns in a stack of driven quasi-one-dimensional dipolar condensates,” (2023), arXiv:2310.11274 [cond-mat.quant-gas].
- [63] S. Müller, J. Billy, E. A. L. Henn, H. Kadau, A. Griesmaier, M. Jona-Lasinio, L. Santos, and T. Pfau, *Phys. Rev. A* **84**, 053601 (2011).
- [64] R. M. Wilson and J. L. Bohn, *Phys. Rev. A* **83**, 023623 (2011).
- [65] L. Du, P. Barral, M. Cantara, J. de Hond, Y.-K. Lu, and W. Ketterle, “Atomic physics on a 50 nm scale: Realization of a bilayer system of dipolar atoms,” (2023), arXiv:2302.07209 [cond-mat.quant-gas].
- [66] D.-W. Wang, M. D. Lukin, and E. Demler, *Phys. Rev. Lett.* **97**, 180413 (2006).
- [67] D.-W. Wang, *Phys. Rev. Lett.* **98**, 060403 (2007).
- [68] C. Trefzger, C. Menotti, and M. Lewenstein, *Phys. Rev. Lett.* **103**, 035304 (2009).
- [69] J. R. Armstrong, N. T. Zinner, D. V. Fedorov, and A. S. Jensen, *Europhysics Letters* **91**, 16001 (2010).
- [70] A. Pikovski, M. Klawunn, G. V. Shlyapnikov, and L. Santos, *Phys. Rev. Lett.* **105**, 215302 (2010).
- [71] D. Hufnagl and R. E. Zillich, *Phys. Rev. A* **87**, 033624 (2013).
- [72] A. Safavi-Naini, S. Söyler, G. Pupillo, H. R. Sadeghpour, and B. Capogrosso-Sansone, *New Journal of Physics* **15**, 013036 (2013).
- [73] M. Rosenkranz, Y. Cai, and W. Bao, *Phys. Rev. A* **88**, 013616 (2013).
- [74] A. Macia, G. E. Astrakharchik, F. Mazzanti, S. Giorgini, and J. Boronat, *Phys. Rev. A* **90**, 043623 (2014).
- [75] F. Cinti, D.-W. Wang, and M. Boninsegni, *Phys. Rev. A* **95**, 023622 (2017).
- [76] A. Boudjemâa and R. Keltoum, *Chaos, Solitons & Fractals* **131**, 109543 (2020).
- [77] S. Bandyopadhyay, H. Sable, D. Gaur, R. Bai, S. Mukerjee, and D. Angom, *Phys. Rev. A* **106**, 043301 (2022).
- [78] N. Bigagli, C. Warner, W. Yuan, S. Zhang, I. Stevenson, T. Karman, and S. Will, *Nature Physics* **19**, 1579 (2023).
- [79] N. Bigagli, W. Yuan, S. Zhang, B. Bulatovic, T. Karman, I. Stevenson, and S. Will, “Observation of bose-einstein condensation of dipolar molecules,” (2023), arXiv:2312.10965 [cond-mat.quant-gas].
- [80] D. Edler, C. Mishra, F. Wächtler, R. Nath, S. Sinha, and L. Santos, *Phys. Rev. Lett.* **119**, 050403 (2017).
- [81] A. Pricoupenko and D. S. Petrov, *Phys. Rev. A* **103**, 033326 (2021).
- [82] T. Bland, E. Poli, L. A. P. n. Ardila, L. Santos, F. Ferlaino, and R. N. Bisset, *Phys. Rev. A* **106**, 053322 (2022).
- [83] S. Li, U. N. Le, and H. Saito, *Phys. Rev. A* **105**, L061302 (2022).
- [84] R. K. Kumar, L. E. Young-S., D. Vudragović, A. Balaž, P. Muruganandam, and S. K. Adhikari, *Computer Physics Communications* **195**, 117 (2015).
- [85] A. de Paz, B. Naylor, J. Huckans, A. Carrance, O. Gorceix, E. Maréchal, P. Pedri, B. Laburthe-Tolra, and L. Vernac, *Phys. Rev. A* **90**, 043607 (2014).
- [86] S. Ronen, D. C. E. Bortolotti, and J. L. Bohn, *Phys. Rev. A* **74**, 013623 (2006).
- [87] A. Griesmaier, J. Werner, S. Hensler, J. Stuhler, and T. Pfau, *Phys. Rev. Lett.* **94**, 160401 (2005).
- [88] Q. Beaufils, R. Chicireanu, T. Zanon, B. Laburthe-Tolra, E. Maréchal, L. Vernac, J.-C. Keller, and O. Gorceix, *Phys. Rev. A* **77**, 061601 (2008).
- [89] K. Aikawa, A. Frisch, M. Mark, S. Baier, A. Rietzler, R. Grimm, and F. Ferlaino, *Phys. Rev. Lett.* **108**, 210401 (2012).
- [90] R. Song, S.-H. Zhang, W.-M. Liao, J. Wang, S.-J. Deng, and H.-B. Wu, *Results in Physics* **52**, 106795 (2023).
- [91] B. Seo, Z. Chen, M. Huang, M. K. Parit, Y. He, P. Chen, and G.-B. Jo, *Journal of the Korean Physical Society* **82**, 901 (2023).
- [92] M. Lu, N. Q. Burdick, S. H. Youn, and B. L. Lev, *Phys. Rev. Lett.* **107**, 190401 (2011).
- [93] A. J. Leggett, *Phys. Rev. Lett.* **25**, 1543 (1970).
- [94] A. Guttridge, D. K. Ruttley, A. C. Baldoock, R. González-Férez, H. R. Sadeghpour, C. S. Adams, and S. L. Cornish, *Phys. Rev. Lett.* **131**, 013401 (2023).